数理物質科学研究科　博士論文の要約

Graduate School of Pure and Applied Sciences

Studies on Polymeric Whispering Gallery Mode Microresonators for Sensing Application

（ポリマーWGM 共振器によるセンシング応用に関する研究）

QIAGEDEER AIRONG

Doctoral program in Materials Science

Student ID: 201730111

Doctor of Philosophy in Engineering

Advised by Yohei Yamamoto

Contents of Thesis

Chapter 1 Introduction

Whispering gallery mode (WGM) optical resonators attract increasing attentions in the field of high precision sensors.[1] WGM resonators confine light via total internal reflection (TIR) at the outermost surface of the resonator. Due to their highly symmetric morphology, spherical WGM resonators in theory exhibit the highest light confinement efficiency among various types of optical resonators. This efficient light confinement strongly enhances light-matter interaction especially at the periphery of the resonator. Therefore, peak positions of the WGM resonance are strongly dependent on the size, geometry and refractive index of the resonator. This spectral feature can be applied to the highly sensitive chemical and physical sensors. And with the great scientific and technological progress today, the focus of these WGM-based sensors is the miniaturization of the sensor systems to further pave the way of portable and remote systems. Polymeric microcavities are feasible for the integration of different kind of active materials into

the polymer matrix in a simple way without using fragile tapered optical fiber. They also possess the advantage of ease of fabrication, low cost and highly flexible. Based on this, polymeric active microcavities are expected to be the promising candidates for the miniaturized WGM based remote sensor in the future.

Chapter 2 Highly sensitive humidity sensor based on aggregation-induced emission luminogen-appended hygroscopic polymer microresonator

Detection of water vapour content in atmosphere is vital in a range of processes including chemical reactions, medical treatments and environmental assessments. Among many types of humidity sensors so far invented, optical sensors are particularly attractive in that its sensor tip and detector can be located without physical connection. Such non-contact configuration enables the humidity detection at physically- or electrically-isolated space. Since the first application of WGM resonators to humidity sensing demonstrated in 2010, several studies have been published which are conventionally built up by using physically tapered tip and detectors, nonetheless such tapered configuration is dispensable for optical sensors. This is presumably because the optical coupling between the taper and resonator is beneficial for enhancing the precision of the optical signals. More recently, non-tapered WGM humidity sensors which are achieved by doping fluorescent dye with hydrophilic polymer have been reported. These sensors consist of tailored resonators that exhibit large spectral peak shift (6-47 pm/% RH) toward a change in humidity. These WGM sensors are advantageous for practical applications because they can be operated with readily available compact laser sources. However, these non-tapered type resonators often suffer from poor luminescence intensity, which is caused primally by the aggregation-caused emission quenching. The chemical incompatibility between the sphere medium and the dopant also poses a limit of the doping concentration. In addition, unlike temperature and pressure sensors, humidity sensors have to uptake the guest water molecules into the resonator medium, which often disrupts the morphology of the sphere or chemical integrity of the constituent polymer. With these situations in mind, we expect that a hydrophilic polymer covalently appended with aggregation-induced emission (AIE) luminogens (AIEgens) will overcome the above difficulties. Namely, the hydrophilic polymer chain will facilitate the swelling of water vapour into the sphere medium, which induces enhanced shift of the resonant peaks upon water sorption. At the same time, the AIEgen exhibits intense luminescence even in the condensed state. To prove this concept, herein we newly synthesize a WGM resonator from an AIEgen-appended hygroscopic polymer and demonstrate its high sensitivity toward humidity.[2] The AIE polymer self-assembles into well-defined microspheres with smooth surface upon sluggish precipitation in binary solution. The photoluminescence (PL) spectra of the microspheres exhibit periodic sharp peaks due to the WGM resonance. The resonant peaks shift toward longer wavelength as the surrounding humidity increases with a sensitivity as high as

255 pm/% RH, which is the highest value among the reported non-tapered optical sensors. The sensitivity toward humidity is virtually intact even after five cycles of absorption and desorption of water vapour.

The molecular structure of AIEgen-appended hygroscopic polymer (**PAA-TPE**) used in this research are shown in Fig.1a. The AIE property of **PAA-TPE** is evident from its appearance under UV illumination (λ_{ex}=365nm). While MeOH solution of **PAA-TPE** is weakly emissive in pale yellow (Fig. 1b), the aqueous suspension and the dried film specimen of **PAA-TPE** emit strong red-orange emission, due to the AIE character (Fig. 1c and d, respectively). A thin film of **PAA-TPE** on a quartz substrate emits orange-red fluorescence with an emission band centred at 606 nm upon photoexcitation (λ_{ex}= 475 nm) with a PL quantum yield of 0.196 (Fig. 1e). Microspherical assemblies of **PAA-TPE** were prepared by interphase precipitation method. Scanning electron microscopic (SEM) images of the precipitated powder show micrometer-scale spherical morphology with average diameter of 3.8 μm (Fig. 1f and g). Analogous to its thin film state, the microspheres of **PAA-TPE** emits orange-red PL with the wavelength centred at 635 nm, upon illumination with blue light (λ_{ex}=460-495 nm, Fig. 1h). PL properties of individual **PAA-TPE** microspheres were investigated by means of μ-PL measurement setup. PL spectrum, obtained upon excitation with focused pulsed laser (λ_{ex} = 470 nm) to a rim of **PAA-TPE** microsphere (d = 3.6 μm), exhibits a sharp and periodic peak set that overlaps on a broad PL band (Fig. 2a). These sharp peaks are attributed to WGM, which originates from a confinement of PL inside the

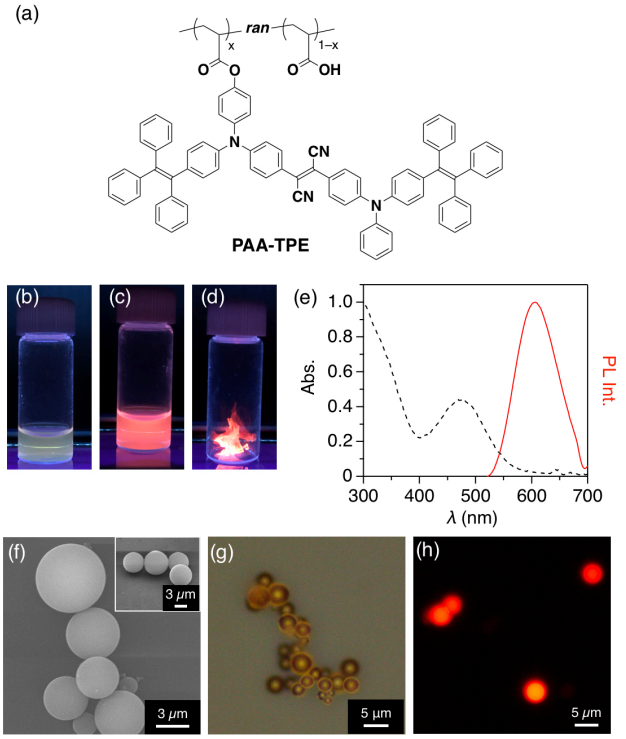

Fig. 1 (a) Molecular structure of **PAA-TPE**. Photographs of a MeOH solution (b) aqueous suspension (c) and dried film (d) of **PAA-TPE** under UV-light illumination at 365 nm. (e) Absorption spectrum of MeOH/H_2O (1/1 v/v) mixed solution of **PAA-TPE** (black curve) and PL spectrum of thin film of **PAA-TPE** drop-casted on a quartz substrate (λ_{ex} = 475 nm). (f) SEM image of **PAA-TPE** microspheres. Optical (g) and fluorescence (h) microscopic images of **PAA-TPE** microspheres.

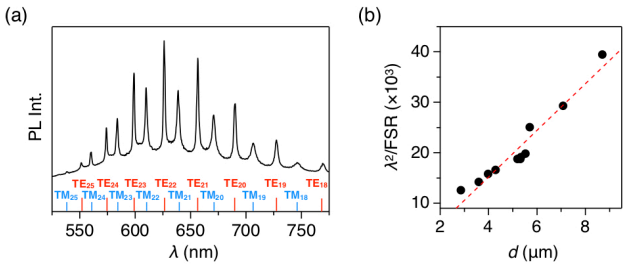

Fig. 2. (a) PL spectrum of a single microsphere of **PAA-TPE** (d = 3.6 μm) upon excitation with pulsed laser (λ_{ex}=470 nm, Δ=70 ps, f =2.5 MHz). Calculated mode numbers of the observed resonant peaks are shown at the bottom. (b) A plot of λ^2/FSR versus d of the **PAA-TPE** microspheres. Dashed line represents the linear fitting of the plot.

microsphere by total internal reflection and self-interfere. A series of the observed peaks are indexed as transverse electric (TE) and magnetic (TM) modes, as shown on the bottom of Figure 2a. **PAA-TPE** microspheres with larger d exhibit analogous PL spectra with narrower free spectral range (FSR), a plot of λ^2/FSR versus d displays a linear correlation (Fig. 2b). The effective refractive index (n_{eff}) is evaluated as 1.47, which is in good agreement with the value obtained by spectroscopic ellipsometry measurement of a cast film of **PAA-TPE** (1.49).

The humidity-dependent μ-PL spectra were shown in Fig. 3. **PAA-TPE** microspheres were drop-cast on a quartz substrate, which was then set onto the top face of a stainless chamber. The chamber was equipped with tubular inlet on the side and outlet holes on the top that allows the humid air to flow. A wireless RH sensor and a small glass dish filled with water were placed together in the chamber. The RH was measured with a time interval of 10 s with ±2% RH accuracy. The humidity was controlled by adjusting the flux of dry nitrogen gas. Single **PAA-TPE** microsphere in the chamber was photoexcited with a focused cw laser (λ_{ex} = 450 nm), and its emission is collected via objective lens. With increasing humidity, resonant peaks of the **PAA-TPE** microsphere (d = 3.7 μm) shifted to the longer wavelength (Fig. 3a). The resonant peak of TM_{24}, for example, shifted by 8.4 nm toward the longer wavelength as the relative humidity increased from 34.6 to 70.3 %RH. The red shift of the resonant peaks results from the increase of d upon swelling. The peak wavelengths of TM_{24} are plotted against the relative humidity, showing a linear relationship with the humidity (Fig. 3b). According to the slope of the plot, the sensitivity of the peak shift against humidity change is 255 pm/ %RH, which is the highest among reported non-tapered optical humidity sensors (6-47 pm/ %RH). The **PAA-TPE** microsphere is tolerant against the multiple cycles of absorption and desorption

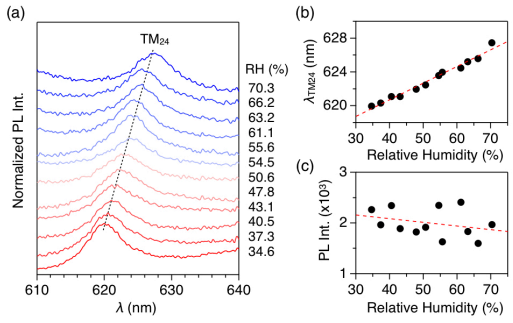

Fig. 3. (a) PL spectra, upon excitation with cw laser (λ_{ex}= 450 nm), of a **PAA-TPE** microsphere (d = 3.7 μm) upon increasing the relative humidity from 34.6 to 70.3 %RH. The dotted line is an eye guide, indicating the peak positions of TM_{24}. (b, c) Plots of the wavelengths (b) and peak intensities (c) of TM_{24} upon increasing the relative humidity from 34.6 to 70.3 %RH.

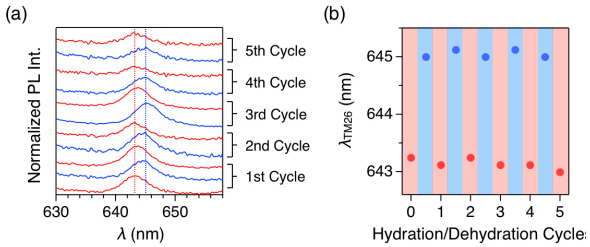

Fig. 4. (a) PL spectra of a **PAA-TPE** microsphere upon increasing and decreasing the surrounding humidity sequentially between 40 (red) and 50 %RH (blue). Red and blue dashed lines indicate the peak position of TM_{26} at 40 and 50 %RH, respectively. (b) Plot of peak wavelengths at TM_{26} versus the number of hydration/dehydration cycles. The red and blue circles indicate the wavelengths of the TM_{26} at 40 and 50 %RH, respectively.

of the water vapour. The repeatability test was carried out with a microsphere (d = 4.1 μm) by switching the surrounding humidity between 40 and 50 %RH with an exposure time of 10 min. The plot of the peak wavelength of TM_{26} against the humidity change displays nearly constant values for each humidity condition upon 5 cycles of the humidity change (Fig. 4a and b). The morphology of the sphere is kept intact through the repeatability test, demonstrating the tolerance of **PAA-TPE** microspheres.

Chapter 3 AIEE-dye doped polymeric microresonator for volatile organic compounds (VOCs) sensing

Besides humidity, volatile organic compounds are also one of the biggest issues need to be detected and monitored in our daily life. In this chapter, a newly synthesized fluorescence compound (***β*-COPV**)[3] which poses an outstanding aggregation induced enhanced emission (AIEE) property was utilized as a doping dye for the fabrication of dye-doped polymeric microresonators. The molecular structure of ***β*-COPV** was shown in Fig. 5a. A $CHCl_3$ solution of ***β*-COPV** emits green fluorescence (Fig. 5c) with an emission band centered at 515 nm upon photoexcitation (λ_{ex}= 355 nm) with a PL quantum yield of 0.41 while a crystal state of ***β*-COPV** exhibits red emission band centered at 607 nm with enhanced PL quantum yield of 0.95 under photoexcitation (Fig.5b). Microspherical assemblies of ***β*-COPV** doped polymer were prepared by interphase precipitation method. SEM images (Fig. 6a) indicate well-defined spherical shape of the obtained ***β*-COPV** doped PS microresonators. The Fluorescence microscopy images indicated that ***β*-COPV** were uniformly dispersed inside the PS matrix showing green emission light (Fig. 6c). When the single microsphere of ***β*-COPV** doped PS with diameter of 5.7 μm was locally excited with a focused pulsed laser beam in air (355 nm, 0.7 ns), a series of resonance peaks were found in the PL spectra collected from the microsphere using various pump pulse energy fluence (P) (Fig. 6d). At lower pumping energy, typical WGM peak was observed, as the pump power increases,

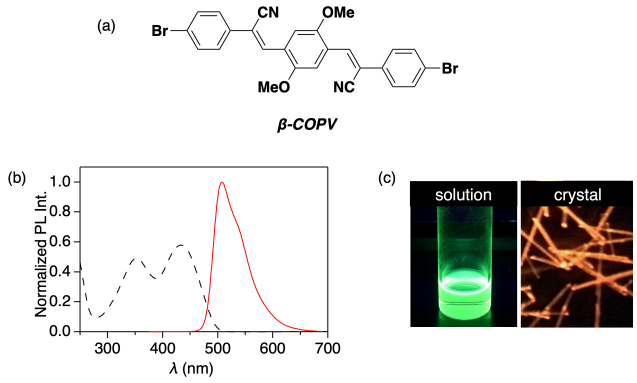

Fig. 5. (a) Molecular structure of ***β*-COPV**. (b) Absorption (dashed curve) and PL spectrum (solid curve) of ***β*-COPV** in $CHCl_3$. (c) Fluorescence microscopic image of ***β*-COPV** in solution and crystal state.

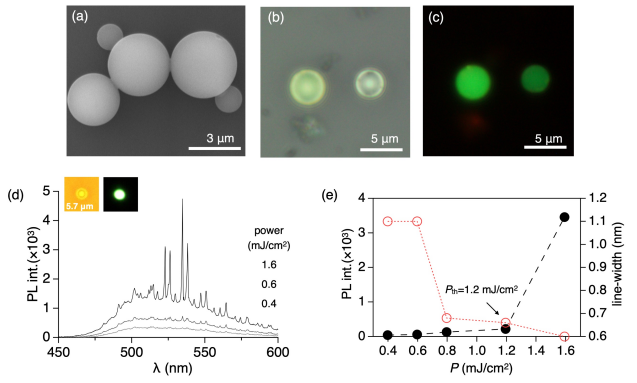

Fig. 6. (a) SEM image of ***β*-COPV** doped PS microspheres. Optical (b) and fluorescence (c) microscopic images of ***β*-COPV** doped PS microspheres (d) PL spectrum of a single microsphere of ***β*-COPV** doped PS polymer (d = 5.7 μm) upon excitation with various pump pulse energy fluence(P) (λ_{ex}= 355 nm, Δ= 0.7 ns). (b) A plot of PL intensity and linewidth versus pump pulse energy fluence (P) of the ***β*-COPV** doped PS microsphere.

several mode peak around 525 nm were selectively and strongly amplified, showing a threshold at 1.2 mJ cm^{-2} (Fig. 6e).

Many polymers exhibit swelling during exposure to organic chemical vapor. The expansion of the polymer during swelling can be exploited to deform an optical cavity. When ***β*-COPV** doped PS microspheres are exposed to the chemical vapor, PS microcavity expands and therefore a change in the optical path length occurred, leading to a shift of the resonance wavelength. The sensing performance of the ***β*-COPV** doped PS microresonators were carried out by applying 8 different volatile organic solvents include ethanol, methanol, THF, acetone, MEK, toluene, benzene and xylene, which are widely reported as the most common VOCs surrounding our daily life. Take Ethanol as an example, when 90 µl of ethanol was injected to the chamber and evaporate naturally, a continuous red-shift during time was recorded and the maximum shift upon 90 µl of ethanol was 8.8 nm. After the shift reaches saturation, pure N_2 was purged into the chamber, in consequence, the ethanol in the microsphere released and the WGMs shift back to their initial position, indicating a good reversibility of this sensing process (Fig. 7a). The sensing performance of ***β*-COPV** doped PS microresonators under exposure to different VOCs were recorded and summarized on chart bar in terms of WGM shift (Fig. 7b). All the measurements show clear shift of WGM peaks upon exposure to chemical vapors, showing excellent versatility. The peak shifts were in the order of MeOH < EtOH < acetone < THF < MEK < *o*-xylene <benzene < toluene. The trend in peak shift can be explained by Hansen solubility parameters (HSP), The geometric distance in the Hansen space (R_a) represents the solubility of two given substances. Namely, when the HSP of a given VOCs is close to that of PS, PS is prone to swell the vapor in a large extent. Fig. 7c shows a plot of peak shift against the R_a value of each VOCs, exhibiting a linear relation. Noteworthy,

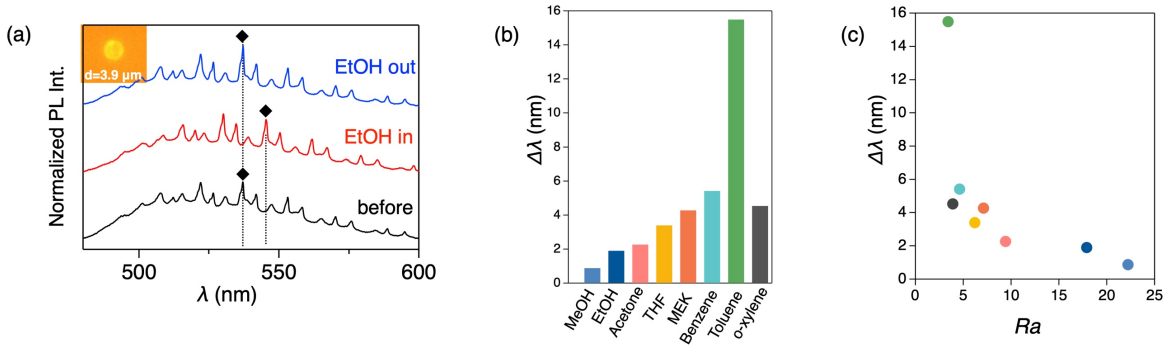

Fig. 7. (a) PL spectra of a single microsphere of ***β*-COPV** doped PS (d = 3.9 µm) upon excitation with pulsed laser (λ_{ex}= 355 nm, 0.7 ns) with exposure to ethanol vapor. (b) The WGMs shift of ***β*-COPV** doped PS microsphere under different volatile organic solvent, which include MeOH, EtOH, Acetone, THF, MEK, Benzene, Toluene and o-xylene. (c) The plot of WGM shift versus Ra in each VOCs.

toluene is the only exception in this trend. The sensitivity toward toluene is far more than those of its analogues such as benzene or *o*-xylene, exhibiting a peculiar selectivity towards toluene.

Chapter 4 Optically switchable microlaser emitter from dye-doped polymeric microresonator

In constructing of ultracompact photonic devices, there emerged an increasing demand for micro/nanoscale lasers that able to perform multiwavelength emitting and wavelength switching.[4] However, in traditional semiconductors, only monochromatic laser output is available because of their continuous energy band structures. Organic materials on the other hand is very helpful for multi wavelength emission/switch due to a series of vibronic peak features. In this chapter, we present a novel wavelength switchable laser based on an excitation power controllable competition of two vibronic lasing band in a dye-doped polymer microresonator. Polystyrene (PS) with the advantage of low absorption losses and ease of processability was selected as the resonator material. The gain medium of a laser strongly influences its performance. In order to obtain low lasing thresholds, an efficient active material needs to be integrated into the resonator without deteriorating the cavity properties. For this purpose, 1,4-bis(2-methylstyryl)benzene (**Bis-MSB**) (Fig. 8a) was found to be the suitable laser dye. Fig. 8b shows the absorption and emission spectra of **Bis-MSB** in polar solvent (ethanol) and non-polar solvent (hexane) respectively, in which a slight shift was observed. The **Bis-MSB** doped PS microspheres were fabricated by mini-emulsion method. Typically, a chloroform solution (0.2 ml) of **Bis-MSB** in PS with desired concentration was added to an H_2O solution of SDS (1.0×10^{-2} M, 2 ml), the two phase-separated solution was emulsified by vigorously stirring with homogenizer (20krpm, 3min). The emulsion was allowed to stand for 2 days in an atmosphere to naturally evaporate chloroform. After removing the excess SDS, a complete precipitation of **Bis-MSB** doped polymer was obtained. SEM images of the precipitated powder show micrometer-scale spherical morphology with smooth surface (Fig. 8c) and emit uniform blue fluorescence light upon excited with 365 nm light (Fig.8d). When the single microsphere of **Bis-MSB** doped PS with diameter of 6.3μm was locally excited with a focused pulsed laser beam in air (355 nm,

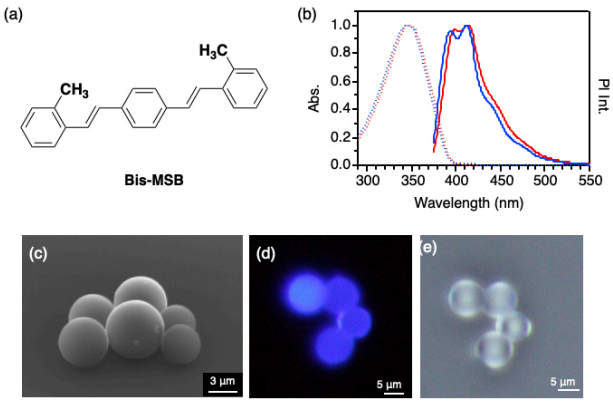

Fig. 8. (a) Molecular structure of laser dye **Bis-MSB**. (b) Absorption (dashed curve) and PL spectrum (solid curve) of **Bis-MSB** in hexane (blue) and ethanol (red) solution. (c) SEM image of **Bis-MSB** doped PS microspheres. Fluorescence (d) and optical (h) microscopic images of **Bis-MSB** doped PS microspheres.

0.7 ns), a series of resonance peaks were found in the PL spectra collected from the microsphere using increased pump pulse energy fluence (*P*) (Fig. 9a). Upon weak excitation, a lasing peak located at 0-2 emission band was observed, as the pump power increases, the lasing peak at longer wavelength disappeared and only the lasing at shorter wavelength dominantly present in 0-1 emission band. The threshold corresponding to the lasing at 461.3 nm and 430.6 nm was estimated to be 24.5 μJ/cm^{2}and 53.2 μJ/cm^2, respectively. (Fig. 9b)

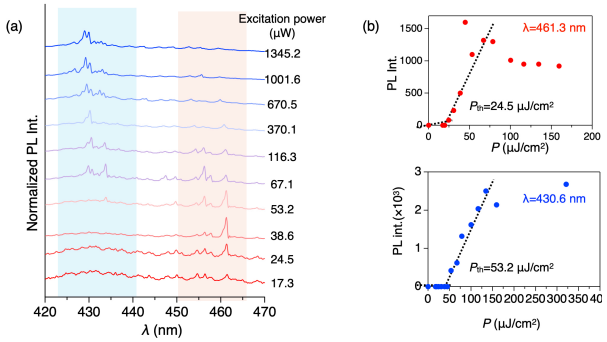

Fig. 9. (a) PL spectrum of a single microsphere of **Bis-MSB** doped PS (d = 6.3 μm) upon excitation with increased pump pulse energy flunce(P) (λ_{ex}= 355 nm, 0.7 ns). (b) A plot of PL intensity versus pump pulse energy fluence (P) of the **Bis-MSB** doped PS microsphere at different wavelength.

More interestingly, a switchable dual-wavelength lasing between 0-1 and 0-2 band was achieved by switching the excitation power. The lasing wavelength switch under excitation power switch was shown in Fig. 10. Under low excitation power of 24.73 μw, the lasing emission only occur at 0-2 band, when a higher excitation power of 34.73 μw was applied, the lasing switched from 460nm to 430 nm and located at 0-1 band. And when the excitation power reduced to 24.73 μm, the lasing peak switched back to 460 nm (0-2 band) again (Fig 10a). This lasing switch behavior under lower and higher excitation power could be repeated more than 10 cycles. Indicating a good reversibility and repeatability (Fig 10b). This switchable lasing behavior upon excitation power change primarily attributed to a competition between optical gain and loss mechanism. The optical propagation loss is much larger at shorter wavelength due to the reabsorption. Therefore, in lower excitation power, due to the larger propagation loss at shorter wavelength than longer wavelength, a lasing action in 0-2 band was activated. However, in higher pumping energy, there is an excitation state absorption behavior induced at around 460 nm, which depressed the lasing emission at 0-2 band and therefore activated the lasing emission at 0-1 band. This competition mechanism of optical gain and loss on switchable lasing behavior provide a new aspect of achieving controllable wavelength switching micro/nano lasers.

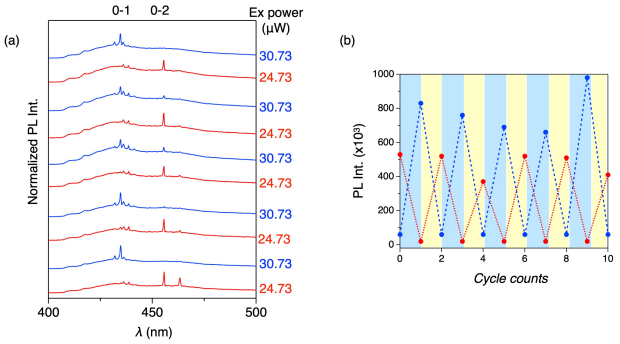

Fig. 10. (a) PL spectrum of lasing switching of a single microsphere of **Bis-MSB** doped PS (d = 7.5 μm) upon excitation with pulsed laser (λ_{ex}= 355 nm, Δ= 0.7 ns) under lower excitation energy (24.73μw) and a higher excitation energy (30.73 μw) (b) Plot of peak intensity at two switchable emission band versus the number of high/low excitation energy cycles. The red and blue circles indicate the lasing band at 460 nm and 430 nm, respectively .

Chapter 5 Conclusions

In summary, polymeric WGM based microresonator as well as their applications in optical sensing either in humidity or VOCs were investigated in this work. In Chapter 2, We successfully fabricated WGM microresonators based on AIEgen-appended hygroscopic polymer, which can be utilized for humidity sensing. The sensitivity of the **PAA-TPE** microsphere toward water vapour reaches 255 pm/%RH, which is the highest among ever reported non-tapered optical humidity sensors. Furthermore, the **PAA-TPE** microsphere maintains its humidity sensing ability through multiple swelling and deswelling cycles. In Chapter 3, a newly synthesised ***β*-COPV** fluorescent compound was successfully doped into a polymer microcavities. This ***β*-COPV** doped polymer microresonator exhibited excellent sensing ability towards a series of volatile organic compounds. With the differences in their solubility parameters, the proposed ***β*-COPV** doped PS microresonators are able to distinguish the kind of organic vapor by monitoring the WGM peak shift, exhibited peculiar toluene selectivity. In chapter 4, organic laser dye **Bis-MSB** was successfully integrated into the polystyrene microcavity, and lasing behaviour in room temperature was achieved and found to be switchable from 0-2 emission band at around 460 nm to 0-1 emission band at around 430 nm upon excitation power increase. Furthermore, reversible test of lasing switching under higher and lower pumping energy was conducted up to 10 cycles showing excellent reversibility and repeatability. We envision that our work of WGM based microresonator sensors open up numerous opportunities for polymeric organic luminogens in the application of miniaturized integrated optical sensing devices for real-time, highly sensitive and reliable sensor.

References

[1] Cai, L., Pan, J., Zhao, Y., Wang, J. & Xiao, S. Whispering Gallery Mode Optical Microresonators: Structures and Sensing Applications, *Phys. Status Solidi Appl. Mater. Sci.* 2020, **217**, 1–18.

[2] A. Qiagedeer, H. Yamagishi, M. Sakamoto, H. Hasebe, F. Ishiwari, T. Fukushima, Y. Yamamoto. A highly sensitive humidity sensor based on an aggregation-induced emission luminogen-appended hygroscopic polymer microresonator, *Mater. Chem. Front.* 2021, **5**, 799-803.

[3] S. Hayashi. Facile investigation of reversible nanostructure changes in flexible crystals, *PREPRINT, 2020,* https://doi.org/10.21203/rs.3.rs-71849/v1

[4] Dong, H. *et al.* Dual-Wavelength Switchable Vibronic Lasing in Single-Crystal Organic Microdisks. *Nano Lett.,* 2017, **17** , 91–96.